



Propagation of heterogeneous and homogeneous planar flames in fuel droplet mists



Qiang Li, Huangwei Zhang*, Chang Shu

Department of Mechanical Engineering, National University of Singapore, 9 Engineering Drive 1, Singapore 117576, Singapore

ARTICLE INFO

Article history:

Received 24 April 2020

Revised 2 August 2020

Accepted 31 August 2020

Available online 6 September 2020

Keywords:

Planar flame

flame propagation

Fuel droplet mists

Droplet evaporation

Propagation speed

Evaporative heat loss

ABSTRACT

Propagation of one-dimensional planar flames laden with fuel droplets is theoretically investigated in this work. Localized homogeneous and heterogeneous flames are considered, characterized by different relative locations of dispersed droplets and propagating flame front. With the assumption of large activation energy for the chemical reaction, correlations describing flame propagation speed, flame temperature, evaporation onset front and completion front are derived. The influences of droplet and fuel properties on propagation of fuel-droplet-laden planar flames are studied. The results indicate that the flames are enhanced under fuel-lean conditions but weakened under fuel-rich conditions. Both effects are intensified with increased droplet mass loading. Fuel vapor and temperature gradient are observed in the post-flame evaporation zone of heterogeneous flames. Evaporation completion front location is considerably affected by the droplet diameter, but the evaporation onset front varies little with droplet properties. Flame bifurcation occurs with high droplet mass loading under fuel-rich mixture, leading to multiplicity of flame propagation speed as well as droplet evaporation onset and completion fronts. Sprayed fuels with larger latent heat of vaporization would weaken the flame enhancement effect under fuel-lean conditions, due to larger evaporation heat loss. Moreover, for homogeneous flames, evaporative heat loss only occurs in the pre-flame zone. However, for heterogeneous flames, heat loss from the post-flame evaporation zone becomes dominant for relatively large droplets. Besides, for fuel-lean mixtures laden with medium-sized fuel droplets, the propagation speed of heterogeneous flames increases with Lewis number, due to the enhanced fuel vapor diffusion in the post-flame zone.

© 2020 Elsevier Ltd. All rights reserved.

1. Introduction

Spray combustion has been widely used in different propulsion systems, e.g. internal combustion engines, gas turbines and liquid rocket engines (Lefebvre and McDonell, 2017). Liquid fuels have numerous advantages, including high energy capacity, easy accessibility and extensive supply sources. Generally, they are injected into the combustors in the form of liquid sheets, and then broken up into smaller droplets to generate fuel sprays or clouds. Efficient droplet evaporation and vapor mixing with the surrounding oxidizer are significant premises for subsequent combustion in gas phase. Due to the intrinsic complexity arising from interphase interactions and high relevance to engineering practice, numerous investigations have been conducted to understand the fundamental aspects of droplet-laden combustion.

The effects of dispersed fuel droplets on flame propagation speed are studied by many researchers. It is found that the flame

speed decreases with increasing liquid fuel loading and droplet size for overall lean and stoichiometric sprays (Ballal and Lefebvre, 1981). Then more effects (e.g. total equivalence ratio or carrier gas velocity) of droplets and oxidizer gas on flame speed are further studied with various hydrocarbon fuels by the same group (Myers and Lefebvre, 1986). Hayashi and Kumagai (1975) observed that the flame speed decreases with fuel loading for lean spray, but increases for rich spray. Nomura et al. (2007, 2000, 1998) found that the flame speed of fuel droplet-vapor-air mixtures exceeds that of premixed gaseous of the same total equivalence ratio in the fuel-lean and fuel-rich regions of the total equivalence ratio. Atzler et al. (2006) observed that the burning rates of iso-octane/air aerosols are markedly affected by droplet diameter only when the equivalence ratio is high. Similar results are also measured by Bradley et al. (2014), through further analyzing equivalence ratio and droplet size effects on flame propagation speed of iso-octane and ethanol aerosols.

Meanwhile, simulations of laminar flame propagation in fuel droplet mists are also available. They can provide supplemental insights about detailed flame and/or droplet dynamics, besides con-

* Corresponding author.

E-mail address: huangwei.zhang@nus.edu.sg (H. Zhang).

firming the relations between flame speed and various properties of two phases in droplet-laden flames. For instance, droplet evaporation behind the flame front may result in reactant stratification and localized diffusion flames (Aggarwal and Sirignano, 1985; Continillo and Sirignano, 1989; Seth et al., 1980). It is also seen by Neophytou and Mastorakos (2009) that with low pressure and temperature, which correspond to the conditions of engine re-light at high altitudes, the effects of pressure and temperature on droplet evaporation are competitive to the gas equivalence ratio and flame speed.

In most of the above studies, how instantaneous distributions of evaporating droplets influence laminar flame propagation is not highlighted. In reality, droplets with large diameters may travel across the flame front to the post-flame zone and continue evaporating there, while small droplets can complete evaporation in the pre-flame zone and the mixture is homogeneous at the flame front. These phenomena have been observed by numerous experimental studies (Sulaiman, 2006; Sulaiman et al., 2007; Thimothee et al., 2017a) and also highlighted by Bradley et al. (2014). However, identifications of the relation between droplet distribution and flame propagation characteristics (e.g. flame speed enhancement) in measurements or simulations are not straightforward due to the comprehensive interphase coupling.

Theoretical analysis is an alternative and attractive method, since it can simplify the problems and retain the most relevant factors in our studies, thereby demonstrating physical relevance and clarity to the large extent. Its success in analyzing two-phase flames can be confirmed by numerous previous work (Greenberg, 2007; Han and Chen, 2016, 2015; Joulin, 1981; Ju and Law, 2000; Li et al., 2020; Lin et al., 1988; Liu and Lin, 1991; Liu et al., 1993; Mitani, 1981; Nicoli et al., 2005; Zhuang and Zhang, 2020, 2019). In particular, Lin and his co-workers (1988, 1991) developed a theoretical model considering the fully and partially pre-vaporized burning sprays. More recently, Belyakov et al. (2018) considered the evaporation onset and completion of water droplets before and behind the flame front, and therefore two flame regimes are obtained with different relations between propagation speed and evaporative heat loss. Later, Zhuang and Zhang (2020) investigated multiplication of propagation speed of spherical flames with water droplets. However, how different distributions of liquid fuel droplets influence two-phase flame propagation are still not well understood.

The present work aims to conduct the theoretical analysis on laminar flame propagation in pre-mixtures laden with fuel droplets, through deriving general theoretical correlations for different flame regimes under both fuel-lean and fuel-rich conditions. The effects of different properties of liquid fuel droplets on planar flame propagation will be discussed, via changing the droplet size, mass loading and latent heat of vaporization. The critical conditions for two flame regimes, i.e. homogeneous and heterogeneous flames, will also be studied. The rest of the paper is structured as below. Mathematical model and theoretical analysis are presented in Sections 2 and 3, respectively. The results from our theoretical analysis will be discussed in Section 4. Section 5 closes the paper with the main conclusions.

2. Physical and mathematical model

2.1. Physical model

In this work, one-dimensional planar flame propagation in a premixed gas with fuel droplet mists will be studied. The schematic of the physical models is shown in Fig. 1. The current model includes four zones, i.e. zones 1–4, to describe the fuel droplet evaporation and fuel vapor combustion. These four zones are demarcated by the evaporation onset front x_v , flame front x_f

and evaporation completion front x_c . It should be noted that, for droplet characteristic locations x_v and x_c , the term “front” is loosely used here to identify where the droplets critically start and finish vaporization. Specifically, x_v corresponds to the location where the droplet starts to evaporate, and the droplets are just heated up to boiling temperature. Behind this front (i.e. $x < x_v$), the droplet temperature maintains the boiling point and evaporation continues (Belyakov et al., 2018; Han and Chen, 2016, 2015; Zhuang and Zhang, 2020, 2019). The evaporation onset front x_v is always before the flame front x_f , indicating that onset of vaporization spatially precedes the gaseous combustion. Moreover, x_c corresponds to the location at which all the droplets are critically vaporized. When $x < x_c$, no droplets are left and hence their effects on the gaseous flame diminish. The reader is reminded that x_v and x_f are determined from our theories as the eigenvalues of the problem, instead of being specified *a priori*. Similar physical models with multiple zones have been successfully used for analyzing droplet-laden laminar flames in previous theoretical analyses (Belyakov et al., 2018; Lin et al., 1988; Zhuang and Zhang, 2020).

Various evaporation dynamics of sprayed fuel droplets and their interactions with gaseous flames may be presented in practical spray combustion. For example, it is observed through experimental measurements (Atzler et al., 2006b; Sulaiman, 2006; Sulaiman et al., 2007; Thimothee et al., 2017a) that droplets with small diameters would complete evaporation in the pre-flame zone or close to the flame front, but relatively large droplets can penetrate through the flame front and continue vaporizing in the post-flame zone. Hence, in the latter scenario, droplets are distributed in the pre-flame zone and part of the post-flame zone.

In our work, both foregoing scenarios will be investigated. Firstly, the evaporation completion front lies after the flame front (i.e. $x_c < x_f$), as shown in Fig. 1(a). In this case, the local mixture around the flame front is heterogeneous, including gas and liquid droplets. Secondly, the evaporation completion front is located before the flame front (i.e. $x_f < x_c < x_v$), and the local mixture around the flame front is purely gaseous and therefore homogeneous, since there all the droplets have been converted into vapor. For brevity, hereafter, we term the first and second cases as heterogeneous and homogeneous flames, respectively. As shown in Figs. 1(a) and 1(b), for both flames, zone 1 represents the pre-vaporization zone before x_v . Zone 2 indicates pre-flame evaporation zone before x_f for heterogeneous flame and before x_c for homogeneous flame. As for zone 3, it represents post-flame evaporation zone before x_c for heterogeneous flame, and pre-flame zone without evaporation for homogeneous flame. Meanwhile, zone 4 is the post-flame zone without evaporation for both flames. In this model, introduction of multiple liquid droplet zones renders it more general, thereby better mimicking practical spray flame problems compared with previous studies (Greenberg et al., 2001; Han and Chen, 2016, 2015).

2.2. Governing equation

For gaseous flames, the well-known diffusive-thermal model (Joulin and Clavin, 1979) is adopted, in which the density and thermal and transport properties (e.g. thermal conductivity and heat capacity) can be assumed to be constant. Gas motion induced by combustion heat release and droplet evaporation is not considered and hence the convection flux is neglected (Han and Chen, 2015; Joulin and Clavin, 1979). This model has been used in numerous previous studies on gaseous and two-phase flame (Chen and Ju, 2007; Han and Chen, 2016, 2015; Li et al., 2020; Zhuang and Zhang, 2020, 2019). One-step chemistry is considered, i.e. $F + O \rightarrow P$, with F , O and P being fuel vapor, oxidizer and product. For completeness, both fuel-lean and fuel-rich conditions for gas composition are studied in this work. Both are relevant in practical droplet-

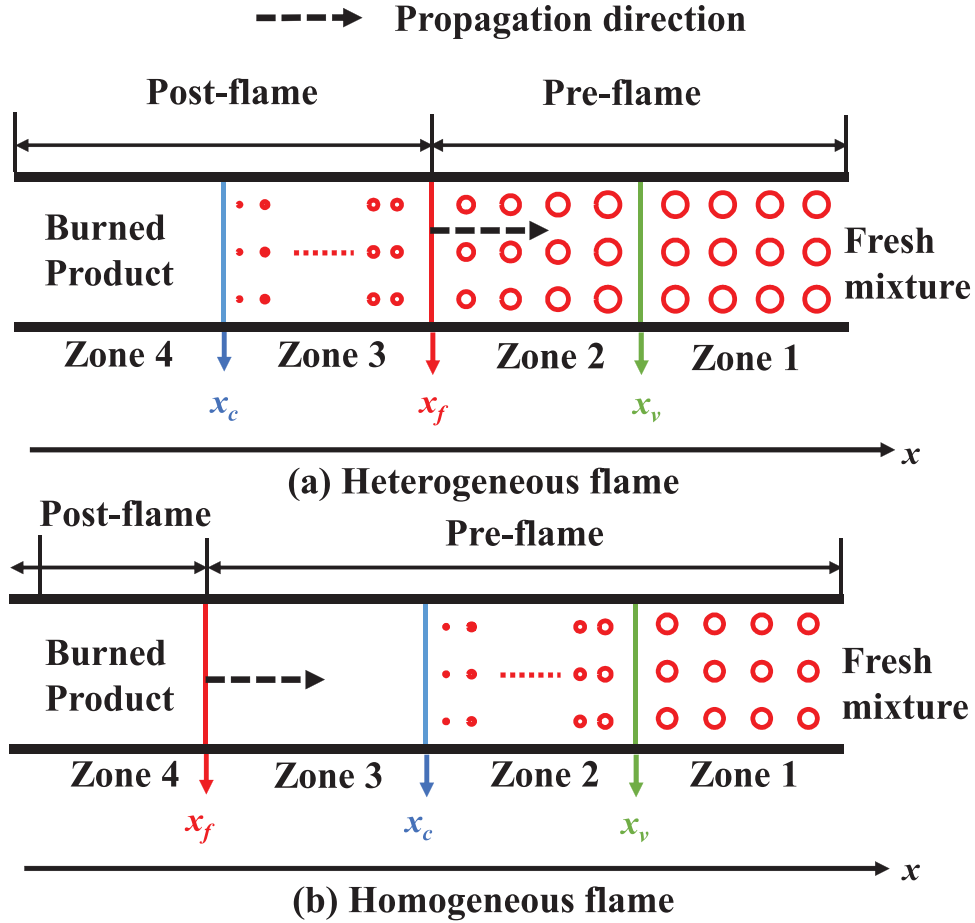


Fig. 1. Schematic of four flame and evaporation zones of laminar planar flames propagating in liquid fuel mists. (a) Heterogeneous flame: droplets complete evaporation in the post-flame zone; (b) Homogeneous flame: droplets complete evaporation in the pre-flame zone. Circles: fuel droplets. x_f : flame front; x_c : droplet evaporation completion front; x_v : droplet evaporation onset front.

laden flame systems, e.g. resulting from various extents of droplet pre-vaporization (Lefebvre and McDonell, 2017).

For liquid fuel droplets, we assume that they are monodispersed in the initial gaseous pre-mixture (Sacmano et al., 2018). The droplets are spherical and their properties (e.g. density and heat capacity) are assumed to be constant. The Eulerian description is adopted for the liquid phase, which is treated as an interpenetrating continuum. Due to the dilute droplet concentration assumption, the inter-droplet collisions are not considered and therefore the diffusion terms in the governing equations for liquid phase can be neglected. Meanwhile, the kinematic equilibrium between two phases is assumed, and droplet dispersion is not considered. The above assumptions for the liquid phase are also used in previous theoretical work on two-phase flames (Blouquin et al., 1997; Ju and Law, 2000; Lin et al., 1988; Blouquin and Joulin, 1995). Furthermore, in zone 1 (pre-vaporization) presented in Fig. 1, thermal equilibrium between droplets and fresh mixture is assumed, and hence they have the same temperature (Belyakov et al., 2018; Han and Chen, 2016, 2015; Zhuang and Zhang, 2020, 2019).

Based on the above assumptions, for the gas phase, the governing equations for temperature, oxidizer and fuel mass fractions are

$$\tilde{\rho}_g \tilde{C}_{p,g} \frac{\partial \tilde{T}}{\partial \tilde{t}} = \tilde{\lambda}_g \frac{\partial}{\partial \tilde{x}} \left(\frac{\partial \tilde{T}}{\partial \tilde{x}} \right) + \tilde{q}_c \tilde{\omega}_c - \tilde{q}_v \tilde{\omega}_v, \quad (1)$$

$$\tilde{\rho}_g \frac{\partial \tilde{Y}_O}{\partial \tilde{t}} = \tilde{\rho}_g \tilde{D}_O \frac{\partial}{\partial \tilde{x}} \left(\frac{\partial \tilde{Y}_O}{\partial \tilde{x}} \right) - \tilde{\omega}_c, \quad (2)$$

$$\tilde{\rho}_g \frac{\partial \tilde{Y}_F}{\partial \tilde{t}} = \tilde{\rho}_g \tilde{D}_F \frac{\partial}{\partial \tilde{x}} \left(\frac{\partial \tilde{Y}_F}{\partial \tilde{x}} \right) - \tilde{\omega}_c + \tilde{\omega}_v, \quad (3)$$

where the upper tilde symbol $\tilde{\cdot}$ is used to indicate that the variables are dimensional. \tilde{t} and \tilde{x} are respectively the time and spatial coordinates, \tilde{T} is the gas temperature. $\tilde{\rho}_g$, $\tilde{C}_{p,g}$, and $\tilde{\lambda}_g$ are the gas density, heat capacity and thermal conductivity, respectively. \tilde{Y} and \tilde{D} are the mass fraction and molecular diffusivity of the gaseous oxidizer or fuel (subscript O for oxidizer, F for fuel), respectively. \tilde{q}_c is the reaction heat release per unit mass of the deficient reactant (oxidizer for fuel-rich case and fuel for fuel-lean case). \tilde{q}_v is the latent heat of vaporization per unit mass of the fuel droplet, and $\tilde{\omega}_v$ is the evaporation rate of the fuel droplet.

The chemical reaction rate $\tilde{\omega}_c$ is assumed to be Arrhenius-type and therefore takes the following form

$$\tilde{\omega}_c = \tilde{\rho}_g \tilde{A} \tilde{Y}_F^\alpha \tilde{Y}_O^{1-\alpha} \exp(-\tilde{E}/\tilde{R}^0 \tilde{T}). \quad (4)$$

Here, α is an indicator for premixture composition, i.e. $\alpha = 1$ for fuel-lean condition and $\alpha = 0$ for fuel-rich condition. Moreover, \tilde{A} is the pre-exponential factor, \tilde{E} is the activation energy for the reaction, and \tilde{R}^0 is the universal gas constant.

The Eulerian equation for droplet mass loading Y_d ($\equiv \tilde{N}_d \tilde{m}_d / \tilde{\rho}_g$) can be derived from single droplet mass equation for \tilde{m}_d and reads (Belyakov et al., 2018; Hayashi and Kumagai, 1975; Zhuang and Zhang, 2020, 2019)

$$\frac{\partial}{\partial \tilde{t}} \left(\frac{\tilde{N}_d \tilde{m}_d}{\tilde{\rho}_g} \right) = \frac{\partial Y_d}{\partial \tilde{t}} = -\frac{\tilde{\omega}_v}{\tilde{\rho}_g}, \quad (5)$$

where \tilde{N}_d is the number density of the droplets.

We assume that the heat transferred from the surrounding gas to the droplets is completely used for phase change, which is related to the latent heat of evaporation \tilde{q}_v (Belyakov et al., 2018; Hayashi and Kumagai, 1975; Zhuang and Zhang, 2020, 2019). Therefore, $\tilde{\omega}_v$ in Eq. (5) can be estimated from the heat transfer rate as

$$\tilde{\omega}_v = \frac{\tilde{N}_d \tilde{s}_d \tilde{h}(\tilde{T} - \tilde{T}_v) H(\tilde{T} - \tilde{T}_v)}{\tilde{q}_v}, \quad (6)$$

where $\tilde{s}_d = \pi \tilde{d}^2$ is the surface area of a single droplet, \tilde{d} is the diameter of the droplet, Nu is the Nusselt number, \tilde{T}_v is the boiling temperature of the fuel droplet. $H(\cdot)$ is the Heaviside function, which indicates that the evaporation process of fuel droplets only exists when the droplets reach the boiling temperature (i.e. when \tilde{x} is between \tilde{x}_c and \tilde{x}_v). \tilde{h} is the heat transfer coefficient, which can be estimated using the following correlation as (Ranz and Marshall, 1952)

$$Nu = \frac{\tilde{h} \tilde{d}}{\tilde{\lambda}_g} = 2.0 + 0.6 Re^{1/2} Pr^{1/3}, \quad (7)$$

where Nu , Pr and Re are the Nusselt number, Prandtl number and particle Reynolds number, respectively. We can neglect the effect of particle Reynolds number Re due to the assumption of kinematic equilibrium and therefore $Nu \approx 2$. Accordingly, the evaporation rate $\tilde{\omega}_v$ in Eq. (5) can be written as

$$\tilde{\omega}_v = \frac{\tilde{N}_d \tilde{s}_d \tilde{\lambda}_g Nu (\tilde{T} - \tilde{T}_v) H(\tilde{T} - \tilde{T}_v)}{\tilde{d} \tilde{q}_v}. \quad (8)$$

The above evaporation model is different from the classic models, e.g. presented in Ref. (Sazhin, 2006). Typically, $\tilde{\omega}_v$ is a function of Sherwood number, Spalding mass transfer number, as well as gas and droplet properties (e.g. density and diameter). In the current study, since we assume that the kinematic equilibrium has been reached between the gaseous and droplet, it can be expected that the effect of the Sherwood number is small. Furthermore, since it is assumed that evaporation proceeds at the boiling temperature and constant atmospheric pressure, the fuel vapor at the droplet surface is relatively constant and hence the Spalding number would change slightly. The difference is that the current model is based on the assumption of energy balance between phase change and heat transfer from the gaseous mixture. In spite of these, it is still physically comprehensive since it considers various effects of the gas and liquid phase properties as mentioned above. Therefore, the current evaporation model is expected to be sufficient. This can also be confirmed by the previous theoretical work using the same model (Belyakov et al., 2018; Zhuang and Zhang, 2020, 2019), from which the physically sound critical flame phenomena have been observed.

To render the analytical analysis in general, Eqs. (1) – (3) can be normalized. As such, the following non-dimensional parameters are introduced

$$U = \frac{\tilde{u}}{\tilde{u}_b}, x = \frac{\tilde{x}}{\tilde{l}_{th}}, t = \frac{\tilde{t}}{\tilde{t}_b}, Y = \frac{\tilde{Y}}{\tilde{Y}_0}, T = \frac{\tilde{T} - \tilde{T}_0}{\tilde{T}_b - \tilde{T}_0}. \quad (9)$$

Here \tilde{T}_0 and \tilde{Y}_0 denote the temperature and fuel mass fraction in the fresh mixture, respectively. \tilde{u}_b , $\tilde{T}_b = \tilde{T}_0 + \tilde{q}_c \tilde{Y}_0 / \tilde{C}_{p,g}$ and $\tilde{l}_{th} = \tilde{D}_{th} / \tilde{u}_b$ are the adiabatic laminar flame speed, temperature and thickness without fuel droplet addition, respectively. $\tilde{D}_{th} = \tilde{\lambda}_g / \tilde{\rho}_g \tilde{C}_{p,g}$ is the thermal diffusivity of the gas phase.

Steady propagation (i.e. $\partial/\partial t = 0$) of planar flames in liquid fuel droplet is assumed, same as Refs. (Belyakov et al., 2018; Lin et al., 1988). Meanwhile, for convenience, our ensuing analysis will be performed in the coordinate system attached to the flame front

$X(t)$, i.e. $\eta = x - X(t)$. Under the above assumption and simplification, the non-dimensional equations of Eqs. (1) – (3) can be written as

$$-U \frac{dT}{d\eta} = \frac{d^2 T}{d\eta^2} + \omega_c - q_v \omega_v, \quad (10)$$

$$-U \frac{d(Y_F Y_O^{1-\alpha})}{d\eta} = \frac{Le_F^{\alpha-1}}{Le_F^\alpha} \frac{d^2(Y_F Y_O^{1-\alpha})}{d\eta^2} - \omega_c + \alpha \omega_v, \quad (11)$$

$$-U \frac{dY_d}{d\eta} = -\omega_v, \quad (12)$$

where $U = dX/dt$ is the non-dimensional flame propagating speed, $q_v = \tilde{q}_v / [\tilde{C}_{p,g}(\tilde{T}_b - \tilde{T}_0)]$ is the normalized latent heat of vaporization, $Le_F = \tilde{D}_{th} / \tilde{D}_F$ and $Le_O = \tilde{D}_{th} / \tilde{D}_O$ are the Lewis numbers of fuel and oxidizer, respectively. In Eq. (11), due to the assumption that the chemical reaction depends on the deficient reactant, for fuel-lean conditions ($\alpha = 1$), we only need to solve the governing equation for the fuel mass fraction Y_F . While in fuel-rich condition ($\alpha = 0$), the oxidizer mass fraction Y_O needs to be solved instead of Y_F . The normalized chemical reaction rate ω_c in Eqs. (10) and (11) reads

$$\omega_c = \frac{Le_O^{\alpha-1}}{Le_F^\alpha} Y_F^\alpha Y_O^{1-\alpha} Z^2 \exp \left[\frac{Z(T-1)}{\sigma + (1-\sigma)T} \right], \quad (13)$$

where Z is the Zel'dovich number, and σ is the thermal expansion ratio.

The non-dimensional droplet evaporation rate ω_v takes the following form

$$\omega_v = \frac{\Omega(T - T_v)}{q_v} H(T - T_v), \quad (14)$$

where T_v is the non-dimensional boiling temperature. The heat exchange coefficient Ω is

$$\Omega = \pi \tilde{N}_d Nu \tilde{d} \tilde{D}_{th}^2 \tilde{u}_b^{-2}. \quad (15)$$

2.3. Jump and boundary conditions

The non-dimensional boundary conditions for both gas phase (T and Y) and liquid phase (Y_d) at the left boundary ($\eta = -\infty$) in the burned zone and the right boundary ($\eta = +\infty$) in the unburned zone can be given as (Belyakov et al., 2018)

$$\eta = -\infty : \frac{dT}{d\eta} = 0, \frac{dY_F}{d\eta} = \frac{dY_O}{d\eta} = 0, Y_d = 0, \quad (16)$$

$$\eta = +\infty : T = 0, Y_F = 1, Y_O = 1, Y_d = \delta. \quad (17)$$

Here δ is the initial mass loading of the fuel droplet in the fresh mixture.

At the evaporation onset front, $\eta = \eta_v$, the gas temperature (T), the mass fractions of oxidizer and fuel (Y_F and Y_O), and the fuel droplet mass loading (Y_d) satisfy the following jump conditions (Belyakov et al., 2018)

$$T = T_v, [T] = [Y_F] = [Y_O] = \left[\frac{dY_F}{d\eta} \right] = \left[\frac{dY_O}{d\eta} \right] = 0, Y_d = \delta. \quad (18)$$

where the square brackets, i.e. $[T] = T(\eta^+) - T(\eta^-)$, denote the difference between the variables at two sides in a particular location.

At the evaporation completion front, $\eta = \eta_c$, the jump conditions for the gas temperature (T), the mass fractions of oxidizer and fuel (Y_F and Y_O), and the fuel droplet mass loading (Y_d) take the following form (Belyakov et al., 2018)

$$\left\{ \begin{aligned} [T] = [Y_F] = [Y_O] &= \left[\frac{dY_F}{d\eta} \right] = \left[\frac{dY_O}{d\eta} \right] = 0, Y_d = 0, \eta_c > 0 \\ [T] = 0, \frac{dT}{d\eta} \Big|_+ &= 0, [Y_d] = 0, \eta_c < 0 \end{aligned} \right. \quad (19)$$

Here, the “+” symbol indicates the value being on the positive side of η_c .

Large activation energy of the gas phase reaction is assumed in this study. This assumption has been successfully used for theoretical analysis of both gaseous (Chen and Ju, 2007; He, 2000; Li et al., 2018; Zhang et al., 2013; Zhang and Chen, 2011) and particle- or droplet-laden (Blouquin et al., 1997; Greenberg, 2007; Han and Chen, 2015; Ju and Law, 2000; Li et al., 2020; Blouquin and Joulin, 1995; Zhuang and Zhang, 2019) flames. It is shown to be adequate to predict main flame dynamics, such as ignition and propagation. In the limit of large activation energy, chemical reaction is confined at an infinitesimally thin flame sheet (i.e. $\eta = 0$) and the jump conditions at the flame front ($\eta = 0$) are

$$T = T_f, Y_F^\alpha Y_O^{1-\alpha} = [Y_d] = 0, \tag{20}$$

$$-\left[\frac{dT}{d\eta}\right] = \frac{Le_0^{\alpha-1}}{Le_F^\alpha} \left[\frac{dY_F^\alpha Y_O^{1-\alpha}}{d\eta}\right] = [\sigma + (1-\sigma)T_f]^2 \exp\left[\frac{Z}{2}\left(\frac{T_f-1}{\sigma+(1-\sigma)T_f}\right)\right], \tag{21}$$

where T_f is the flame temperature.

3. Analytical solution

Eqs. (10)–(12) with boundary and jump conditions (i.e. Eqs. (16)–(21)) can be solved analytically. The distributions of the gas temperature T , fuel mass fraction Y_F (fuel-lean condition), oxidizer mass fraction Y_O (fuel-rich condition) and droplet mass loading Y_d in four zones and the correlations for the flame speed U , flame temperature T_f , evaporation onset front η_v and evaporation completion front η_c are presented below.

3.1. Distributions of T , $Y_{[F, O]}$ and Y_d

The distributions for temperature T from zone 1 to 4 are (the number subscript for T indicates the corresponding zone, which also applies for other variables hereafter)

$$T_1(\eta) = \frac{T_v e^{-U\eta}}{e^{-U\eta_v}}, \tag{22}$$

$$T_2(\eta) = T_v + \frac{UT_v}{\gamma_b - \gamma_a} [e^{\gamma_a(\eta-\eta_v)} - e^{\gamma_b(\eta-\eta_v)}], \tag{23}$$

$$T_3(\eta) = \begin{cases} \frac{T_v}{\gamma_b - \gamma_a} [\gamma_a e^{\gamma_a(\eta_c - \eta_v)} - \gamma_b e^{\gamma_b(\eta_c - \eta_v)}] [1 - e^{-U(\eta - \eta_c)}] + T_v \\ + \frac{UT_v}{\gamma_b - \gamma_a} [e^{\gamma_a(\eta_c - \eta_v)} - e^{\gamma_b(\eta_c - \eta_v)}], \eta_c > 0 \\ T_v + \frac{T_f - T_v}{\frac{e^{-\gamma_b\eta_c}}{\gamma_b} - \frac{e^{-\gamma_a\eta_c}}{\gamma_a}} \left[\frac{e^{\gamma_b(\eta - \eta_c)}}{\gamma_b} - \frac{e^{\gamma_a(\eta - \eta_c)}}{\gamma_a} \right], \eta_c < 0 \end{cases}, \tag{24}$$

$$T_4(\eta) = \begin{cases} T_f, \eta_c > 0 \\ T_v + \frac{T_f - T_v}{\frac{e^{-\gamma_b\eta_c}}{\gamma_b} - \frac{e^{-\gamma_a\eta_c}}{\gamma_a}} \left(\frac{1}{\gamma_b} - \frac{1}{\gamma_a} \right), \eta_c < 0 \end{cases}, \tag{25}$$

where $\gamma_{a,b} = 0.5[-U \pm \sqrt{4\Omega + U^2}]$.

Substituting the temperature distribution into the droplet mass loading equation, we can obtain the distribution of the droplet mass loading Y_d as

$$Y_{d,1}(\eta) = \delta, \tag{26}$$

$$Y_{d,2}(\eta) = \begin{cases} \left[\frac{\Omega T_v}{q_v(\gamma_b - \gamma_a)} \left[\frac{e^{\gamma_a(\eta - \eta_v)} - e^{\gamma_a(\eta_c - \eta_v)}}{\gamma_a} - \frac{e^{\gamma_b(\eta - \eta_v)} - e^{\gamma_b(\eta_c - \eta_v)}}{\gamma_b} \right], \eta_c > 0 \\ \delta + \frac{\Omega T_v}{q_v(\gamma_b - \gamma_a)} \left[\frac{e^{\gamma_a(\eta - \eta_v)} - 1}{\gamma_a} - \frac{e^{\gamma_b(\eta - \eta_v)} - 1}{\gamma_b} \right], \eta_c < 0 \end{cases}, \tag{27}$$

$$Y_{d,3}(\eta) = \begin{cases} 0, \eta_c > 0 \\ \frac{\Omega(T_f - T_v)}{Uq_v \left(\frac{e^{-\gamma_b\eta_c}}{\gamma_b} - \frac{e^{-\gamma_a\eta_c}}{\gamma_a} \right)} \left[\frac{e^{\gamma_b(\eta - \eta_c)} - 1}{\gamma_b^2} - \frac{e^{\gamma_a(\eta - \eta_c)} - 1}{\gamma_a^2} \right], \eta_c < 0 \end{cases}, \tag{28}$$

$$Y_{d,4}(\eta) = 0. \tag{29}$$

The distributions of fuel mass fraction Y_F (fuel-lean condition), oxidizer mass fraction Y_O (fuel-rich condition) can be obtained by solving Eq. (11) with the temperature distributions (i.e. Eqs. (22)–(25)) in the respective zones. For the fuel-lean condition ($\alpha = 1$), fuel mass fraction distributions in four zones are

$$Y_{F,1}(\eta) = \begin{cases} \left[\frac{\frac{I_2'(\eta_v)}{I_1'(\eta_v)}(I_1(0) - I_1(\eta_v)) - \frac{I_2'(\eta_c)}{I_1'(\eta_c)}(I_1(0) - I_1(\eta_c)) + I_2(\eta_v) - I_2(\eta_c) - 1}{I_1(0)} \right] \\ I_1(\eta) + 1, \eta_c > 0 \\ \frac{\frac{I_2'(\eta_v)}{I_1'(\eta_v)}(I_1(0) - I_1(\eta_v)) - 1 + I_2(\eta_v) - I_2(0)}{I_1(0)} I_1(\eta) + 1, \eta_c < 0 \end{cases}, \tag{30}$$

$$Y_{F,2}(\eta) = \begin{cases} 1 - \left[\frac{1 + \frac{I_2'(\eta_v)}{I_1'(\eta_v)} I_1(\eta_v) + \frac{I_2'(\eta_c)}{I_1'(\eta_c)} (I_1(0) - I_1(\eta_c)) - I_2(\eta_v) + I_2(\eta_c)}{I_1(0)} \right] I_1(\eta) \\ + I_2(\eta) + \frac{I_2'(\eta_v)}{I_1'(\eta_v)} I_1(\eta_v) - I_2(\eta_v), \eta_c > 0 \\ 1 - \frac{\frac{I_2'(\eta_v)}{I_1'(\eta_v)} I_1(\eta_v) + 1 - I_2(\eta_v) + I_2(0)}{I_1(0)} I_1(\eta) + I_2(\eta) \\ + \frac{I_2'(\eta_v)}{I_1'(\eta_v)} I_1(\eta_v) - I_2(\eta_v), \eta_c < 0 \end{cases}, \tag{31}$$

$$Y_{F,3}(\eta) = \begin{cases} \left[1 + \frac{I_2'(\eta_v)}{I_1'(\eta_v)} I_1(\eta_v) - \frac{I_2'(\eta_c)}{I_1'(\eta_c)} I_1(\eta_c) - I_2(\eta_v) + I_2(\eta_c) \right] \\ \left[1 - \frac{I_1(\eta)}{I_1(0)} \right], \eta_c > 0 \\ \frac{I_2'(\eta_c)}{I_1'(\eta_c)} [I_1(0) - I_1(\eta)] + I_3(\eta) - I_3(0), \eta_c < 0 \end{cases}, \tag{32}$$

$$Y_{F,4}(\eta) = \begin{cases} 0, \eta_c > 0 \\ \frac{I_2'(\eta_c)}{I_1'(\eta_c)} [I_1(0) - I_1(\eta_c)] + I_3(\eta_c) - I_3(0), \eta_c < 0 \end{cases}, \tag{33}$$

where $I_1'(\eta)$, $I_2'(\eta)$ and $I_3'(\eta)$ are respectively the first order derivatives of $I_1(\eta)$, $I_2(\eta)$ and $I_3(\eta)$, which read

$$I_1(\eta) = \frac{e^{-Le_F U \eta}}{Le_F U}, \tag{34}$$

$$I_2(\eta) = -\frac{Le_F \Omega T_v U}{q_v(\gamma_b - \gamma_a)} \left[\frac{e^{\gamma_a(\eta - \eta_v)}}{\gamma_a(Le_F U + \gamma_a)} - \frac{e^{\gamma_b(\eta - \eta_v)}}{\gamma_b(Le_F U + \gamma_b)} \right], \tag{35}$$

$$I_3(\eta) = -\frac{Le_F \Omega (T_f - T_v)}{q_v \left(\frac{e^{-\gamma_b\eta_c}}{\gamma_b} - \frac{e^{-\gamma_a\eta_c}}{\gamma_a} \right)} \left[\frac{e^{\gamma_b(\eta - \eta_c)}}{\gamma_b^2(Le_F U + \gamma_b)} - \frac{e^{\gamma_a(\eta - \eta_c)}}{\gamma_a^2(Le_F U + \gamma_a)} \right]. \tag{36}$$

For fuel-rich condition ($\alpha = 0$), oxidizer mass fraction distributions in the four zones are

$$Y_{0,12}(\eta) = 1 - e^{-Le_0 U \eta}, \quad (37)$$

$$Y_{0,3}(\eta) = \begin{cases} 1 - e^{-Le_0 U \eta}, & \eta_c > 0 \\ 0, & \eta_c < 0 \end{cases}, \quad (38)$$

$$Y_{0,4}(\eta) = 0. \quad (39)$$

3.2. Correlations for propagating planar flame with fuel droplets

The correlations between the flame propagating speed U , flame temperature T_f , evaporation onset front η_v and evaporation completion front η_c can be derived based on jump conditions at the flame front, i.e. Eq. (21).

3.2.1. Heterogeneous flame

When the flame propagates in the locally heterogeneous mixture, the correlation $\mathcal{F}(U, T_f, \eta_v, \eta_c) = 0$ takes the following form

$$\frac{T_f - T_v}{\frac{e^{-\gamma_b \eta_c}}{\gamma_b} - \frac{e^{-\gamma_a \eta_c}}{\gamma_a}} [e^{-\gamma_b \eta_c} - e^{-\gamma_a \eta_c}] - \frac{UT_v}{\gamma_b - \gamma_a} [\gamma_a e^{-\gamma_a \eta_v} - \gamma_b e^{-\gamma_b \eta_v}] = Q(T_f) \quad (40)$$

$$\begin{cases} U(1 + \delta) + \frac{\Omega(T_f - T_v)}{q_v \left(\frac{e^{-\gamma_b \eta_c}}{\gamma_b} - \frac{e^{-\gamma_a \eta_c}}{\gamma_a} \right)} H(\eta_c) = Q(T_f), & \alpha = 1 \\ U = Q(T_f), & \alpha = 0 \end{cases}, \quad (41)$$

$$T_v + \frac{UT_v}{\gamma_b - \gamma_a} [e^{-\gamma_a \eta_v} - e^{-\gamma_b \eta_v}] = T_f, \quad (42)$$

$$\begin{aligned} & \frac{\Omega(T_f - T_v)}{U q_v \left(\frac{e^{-\gamma_b \eta_c}}{\gamma_b} - \frac{e^{-\gamma_a \eta_c}}{\gamma_a} \right)} \left[\frac{e^{-\gamma_b \eta_c} - 1}{\gamma_b^2} - \frac{e^{-\gamma_a \eta_c} - 1}{\gamma_a^2} \right] \\ & = \delta + \frac{\Omega T_v}{q_v (\gamma_b - \gamma_a)} \left[\frac{e^{-\gamma_a \eta_v} - 1}{\gamma_a} - \frac{e^{-\gamma_b \eta_v} - 1}{\gamma_b} \right], \end{aligned} \quad (43)$$

where

$$Q(T_f) = [\sigma + (1 - \sigma)T_f]^2 \exp \left[\frac{Z}{2} \left(\frac{T_f - 1}{\sigma + (1 - \sigma)T_f} \right) \right], \quad (44)$$

$$H(\eta_c) = \frac{\gamma_b (1 - e^{LeU \eta_c}) + LeU (1 - e^{-\gamma_b \eta_c})}{\gamma_b^2 (\gamma_b + LeU)} - \frac{\gamma_a (1 - e^{LeU \eta_c}) + LeU (1 - e^{-\gamma_a \eta_c})}{\gamma_a^2 (\gamma_a + LeU)}. \quad (45)$$

3.2.2. Homogeneous flame

When the liquid droplets are fully vaporized ahead of the flame front, the correlation $\mathcal{F}(U, T_f, \eta_v, \eta_c) = 0$ reads

$$-\frac{UT_v}{\gamma_b - \gamma_a} [\gamma_a e^{\gamma_a (\eta_c - \eta_v) + U \eta_c} - \gamma_b e^{\gamma_b (\eta_c - \eta_v) + U \eta_c}] = Q(T_f), \quad (46)$$

$$\begin{cases} U(1 + \delta) = Q(T_f), & \alpha = 1 \\ U = Q(T_f), & \alpha = 0 \end{cases}, \quad (47)$$

$$\frac{T_v}{\gamma_b - \gamma_a} \{ (\gamma_a + U - \gamma_a e^{U \eta_c}) e^{\gamma_a (\eta_c - \eta_v)} - (\gamma_b + U - \gamma_b e^{U \eta_c}) e^{\gamma_b (\eta_c - \eta_v)} \} + T_v = T_f, \quad (48)$$

$$\frac{\Omega T_v}{q_v (\gamma_b - \gamma_a)} \left[\frac{1 - e^{\gamma_a (\eta_c - \eta_v)}}{\gamma_a} - \frac{1 - e^{\gamma_b (\eta_c - \eta_v)}}{\gamma_b} \right] = \delta. \quad (49)$$

For homogeneous flames, when $\delta \rightarrow 0$ and $\Omega \rightarrow 0$, the correlations from our model can recover that for purely gaseous planar

flames in Ref. (Chen and Ju, 2007), which is shown in Supplementary Material.

Through solving the above systems $\mathcal{F}(U, T_f, \eta_v, \eta_c) = 0$, we can analyze the relations between the droplets properties (i.e. evaporation onset and completion fronts, η_v and η_c) and flame propagation properties (e.g. flame speed U and temperature T_f), subject to various droplet parameters (e.g. droplet diameter and mass loading, latent heat of vaporization). Thus, propagation of heterogeneous and homogeneous flames with fuel droplets can be analyzed theoretically.

3.3. Critical condition between heterogeneous and homogeneous flames

The critical condition between heterogeneous and homogeneous flames can be derived from the current model when the evaporation completion front coincides with the flame front, i.e. $\eta_c \rightarrow 0$. This physically corresponds to the case in which the liquid fuel droplets are just fully vaporized at the flame front. Practically, it may occur when the droplet diameter is small or the latent heat of vaporization is low (Atzler et al., 2006; Thimothée et al., 2017b). In this case, the correlations for flame propagating speed U , flame temperature T_f and evaporation onset front η_v read

$$-\frac{UT_v}{\gamma_b - \gamma_a} [\gamma_a e^{-\gamma_a \eta_v} - \gamma_b e^{-\gamma_b \eta_v}] = Q(T_f), \quad (50)$$

$$\begin{cases} U(1 + \delta) = Q(T_f), & \alpha = 1 \\ U = Q(T_f), & \alpha = 0 \end{cases}, \quad (51)$$

$$T_v + \frac{UT_v}{\gamma_b - \gamma_a} [e^{-\gamma_a \eta_v} - e^{-\gamma_b \eta_v}] = T_f, \quad (52)$$

$$\delta + \frac{\Omega T_v}{q_v (\gamma_b - \gamma_a)} \left[\frac{e^{-\gamma_a \eta_v} - 1}{\gamma_a} - \frac{e^{-\gamma_b \eta_v} - 1}{\gamma_b} \right] = 0. \quad (53)$$

4. Results and discussion

In this Section, analysis on propagation of one-dimensional planar flames laden with fuel droplets will be conducted based on the correlations derived in Section 3. Zel'dovich number Z and thermal expansion ratio σ are set to be $Z = 10$ and $\sigma = 0.15$, following the values used in previous theoretical analysis (Chen and Ju, 2007; Han and Chen, 2016, 2015; Li et al., 2020; Zhuang and Zhang, 2020, 2019). The non-dimensional boiling temperature T_v is assumed to be $T_v = 0.15$ (Han and Chen, 2015; Lefebvre and McDonell, 2017), which can represent the boiling temperature of most liquid hydrocarbon fuels.

4.1. Effects of droplet diameter and mass loading

Fig. 2 shows the flame speed U and temperature T_f as functions of the initial droplet diameter d_0 , under fuel-lean conditions. The normalized latent heat of vaporization q_v is assumed to be 0.4 in this Section, corresponding to typical liquid hydrocarbon fuels (e.g. ethanol) (Lefebvre and McDonell, 2017). Note that each curve corresponds to a fixed initial droplet mass loading δ . For fuel-lean results in Fig. 2(a) and 2(b), when d_0 is small ($< 30 \mu\text{m}$), the flames are kinetically enhanced, parameterized by higher propagation speed and flame temperature, compared with the droplet-free gaseous mixture (i.e. $U = 1$ and $T_f = 1$). This is caused by the fuel vapors from droplet evaporation, which enrich the gas mixture towards stoichiometry. This kinetic enhancement dominates the thermal weakening effects through evaporative heat loss for this range of droplet sizes. Meanwhile, the net enhancement effects become more pronounced with decreased d_0 , due to the faster evaporation rate of smaller droplets. This is also observed through the

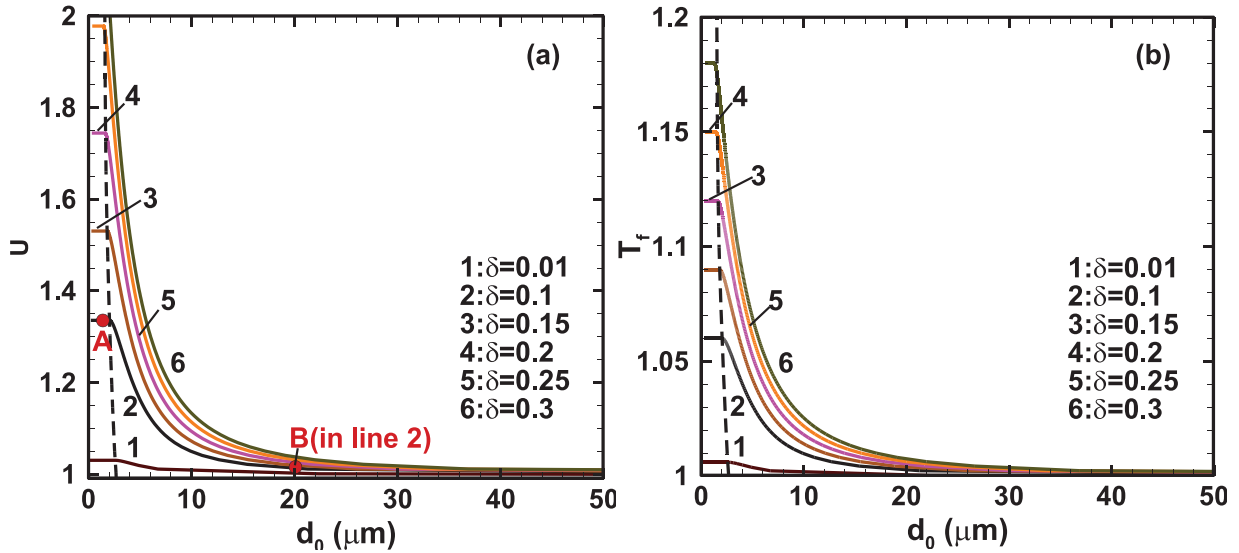


Fig. 2. Effect of droplet diameter and mass loading under fuel-lean conditions: (a) propagation speed, (b) flame temperature. Homogeneous (heterogeneous) flames: left (right) to the dashed flame regime line.

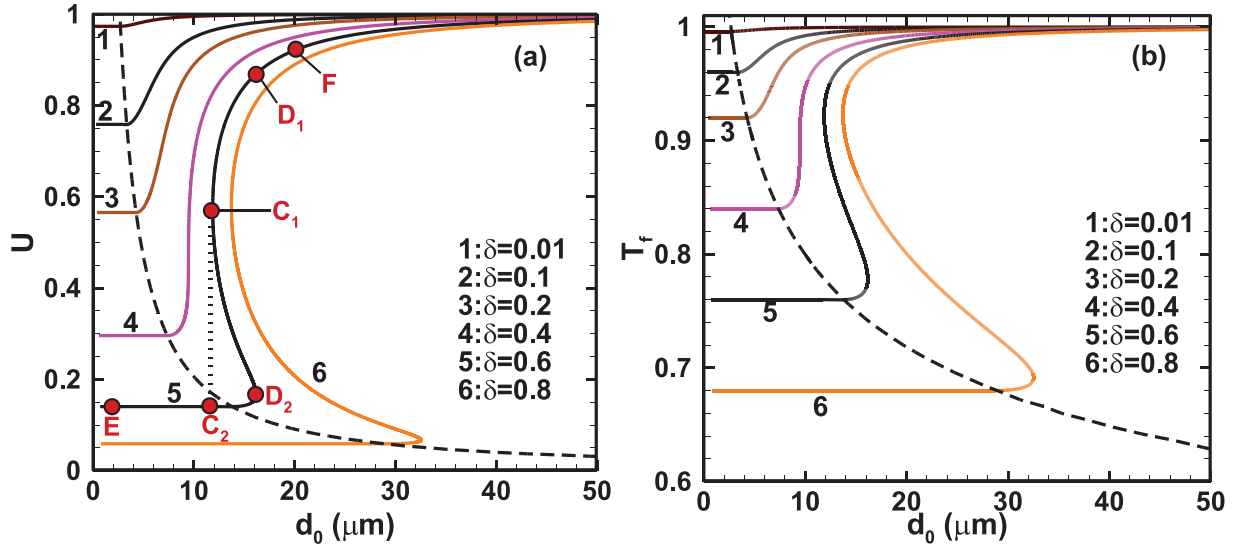


Fig. 3. Effect of droplet diameter and mass loading under fuel-rich conditions: (a) propagation speed, (b) flame temperature. Homogeneous (heterogeneous) flames: left (right) to the dashed flame regime line.

theoretical analysis (Lin et al., 1988; Lin and Sheu, 1991) and numerical simulations (Neophytou and Mastorakos, 2009) of laminar flame propagation in dilute fuel sprays. Furthermore, for a fixed d_0 less than $30 \mu\text{m}$, the higher the mass loading δ , the higher the propagation speed U . This is justifiable since more fuels would be vaporized from the liquid phase. When d_0 is large ($> 30 \mu\text{m}$), the effects of d_0 on the propagating flames are negligible, as seen from Figs. 2(a) and 2(b), since the fuel droplet with larger d_0 has slower evaporation rate.

The fuel-rich flame results are shown in Figs. 3(a) and 3(b). It should be highlighted that, different from the above fuel-lean cases, the kinetic effects from the fuel vapor would weaken the flame, through rendering the originally fuel-rich gas mixture more off-stoichiometric. As such, this kinetic weakening, together with the heat loss from droplet evaporation, is responsible for much lower flame speed and temperature than those of droplet-free cases (i.e. $U = 1$ and $T_f = 1$). This is particularly obvious for small-sized droplets (i.e. $d_0 \leq 40 \mu\text{m}$, see Figs. 3a and 3b). For large droplets (e.g. $d_0 > 40 \mu\text{m}$), the kinetic weakening effects on flame

propagation speed and temperature become marginal, similar to the findings from large droplets in fuel-lean cases in Fig. 2(a) and 2(b). In general, the tendencies of flame speeds with droplet size and mass loading in both fuel-lean and -rich situations (see Figs. 2 and 3) are qualitatively consistent with the previously theoretical analysis (Lin et al., 1988) and experimental measurements (Ballal and Lefebvre, 1981; Hayashi et al., 1977; Hayashi and Kumagai, 1975).

Moreover, in fuel-rich cases, when the initial mass loading δ is small or intermediate, i.e. $\delta \leq 0.2$, $U - d_0$ and $T_f - d_0$ curves are monotonic, and smaller d_0 would lead to lower flame speed and temperature, closer to the results of droplet-free flames, due to both kinetic and thermal weakening effects caused by droplet evaporation. However, when δ is large, i.e. $\delta \geq 0.6$ in Fig. 3, $U - d_0$ and $T_f - d_0$ curves become S-shaped, and multiplicity of the flame propagation speed and temperature is observed. Similar bifurcation is also found in theoretical analysis of premixed planar flames with water or fuel droplets (Belyakov et al., 2018; Lin et al., 1988; Zhuang and Zhang, 2020) and solid particles (Ju and Law, 2000;

Table 1
Conditions of selected flames in Figs. 2(a) and 3(a).

Flame	Condition	d_0 (μm)	q_v	δ
A	Fuel-lean	2	0.4	0.1
B	Fuel-lean	20	0.4	0.1
C	Fuel-rich	11.5	0.4	0.6
D	Fuel-rich	16.1	0.4	0.6
E	Fuel-rich	2	0.4	0.6
F	Fuel-rich	20	0.4	0.6

Li et al., 2020). There are three branches for these cases, e.g. $\delta = 0.6$ in Figs. 3(a) and 3(b): upper stable strong flame (branch above C_1 , indicated in Fig. 3a), middle unstable flame (branch between C_1 and D_2), and lower stable weak flame (branch left to D_2). A detailed linear stability analysis is provided in the Supplementary Material. Slight increase of d_0 around the turning point D_2 would make this weak flame jump to a stronger flame D_1 . Likewise, sudden transition would occur from strong flame C_1 to weak flame C_2 when d_0 is perturbed towards a reduced value. These changes between different flames indicate the re-establishment of the balance between the foregoing kinetic and thermal effects caused by the dispersed liquid phase.

The results of a constant mass loading δ , i.e. each curve in both Figs. 2 and 3, correspond to two flame regimes, i.e. heterogeneous and homogeneous flames, depending on the relative locations of the droplet distribution and flame front, as described in Section 2.1. They are demarcated by dashed lines calculated from Eqs. (50) – (53), and the homogeneous (heterogeneous) flames lie left (right) of the $U - d_0$ or $T_f - d_0$ plane to these lines (termed as flame regime line hereafter). In general, homogeneous flames only exist when d_0 is relatively small. This is reasonable because small droplets are more prone to complete evaporation before the flame front arrives, due to comparatively fast evaporation. As such, the local mixture immediately before the flame front is purely gaseous. Meanwhile, U and T_f of homogeneous flames for a fixed mass loading remain constant, since the same amount of the fuel is vaporized into the mixture. However, for heterogeneous flames, different tendencies are observable for fuel-lean and fuel-rich conditions as presented in Figs. 2 and 3, which have been discussed above. This indicates the strong effects of the initial droplet diameter and mass loading on propagation of heterogeneous flames, which will be further discussed later. It should also be highlighted that flame bifurcations can occur within the same flame regime (from D_2 to D_1 in heterogeneous regime), or between the different flame regimes (from heterogeneous C_1 to homogeneous C_2).

Distributions of gas temperature T , deficient species mass fraction, Y_F or Y_O , and droplet mass loading Y_d of different droplet-laden flames are shown in Fig. 4. For reference, the locations of evaporation onset and completion fronts, i.e. η_v and η_c , are also shown. Four flames are considered, i.e. A, B, E, and F, which are denoted in Figs. 2(a) or 3(a). Flames A and B are under fuel-lean condition. Specifically, A is a homogeneous flame (initial droplet size $d_0 = 2 \mu\text{m}$), while B ($d_0 = 20 \mu\text{m}$) corresponds to a heterogeneous one. For flame A in Fig. 4(a), the droplets are fully vaporized (i.e. $Y_d \rightarrow 0$) slightly before the flame front, and therefore all of them are consumed in the flame. The extra fuel vapor from droplet evaporation increases the overall fuel concentration in the gaseous mixture, leading to slightly higher temperature (i.e. $T > 1$) in the post-flame zone compared to the droplet-free flame. Meanwhile, due to no droplets ($Y_d = 0$) in the post-flame zone, the local evaporative heat loss is zero, and hence the local temperature T is uniform and no temperature gradient exists in the burned zone. Therefore, in homogeneous flames, the thermal effects discussed

in Fig. 2, i.e. heat loss from evaporation of liquid fuel droplets, are only present in the pre-flame zone.

The structure of heterogeneous flame B in Fig. 4(b) is different from that of flame A. Firstly, finite values of fuel mass fraction Y_F can be found in the post-flame zone (i.e. $\eta < 0$), due to evaporation of the penetrated droplets. Part of them contribute towards the flame through the back diffusion from the post-flame zone to the flame front, which is also observed from the one-dimensional simulations of propagating flame in fuel mists (Aggarwal and Sirignano, 1985). However, there are still finite residual fuel vapors beyond the evaporation zone in the burned area, i.e. $\eta < \eta_c$. This is different from the results in flame A, and the kinetic effects of flame B arise from both pre- and post-flame evaporation zones. Secondly, the gas temperature in the post-flame zone gradually decreases from the flame front in the post-flame evaporation zone. Heat conduction in this zone (i.e. $\eta_c < \eta < 0$) would also weaken the flame reactivity, due to the considerable temperature gradient near the flame front. This is also observed from the results of laminar premixed flame with water mists (Belyakov et al., 2018). Therefore, the thermal effects on heterogeneous flames include evaporative heat loss in the pre- and post-flame evaporation zones and also heat conduction in the post-flame evaporation zone.

For fuel-rich condition, the structures of flames E and F are shown in Figs. 4(c) and 4(d), respectively. Note that mass fraction of oxidizer Y_O , instead of Y_F , is shown here. As seen from Fig. 3(a), flame E is from the lower branch ($d_0 = 2 \mu\text{m}$) and a homogeneous flame. However, flame F lies at the upper branch (initial droplet diameter $d_0 = 20 \mu\text{m}$) and hence is a heterogeneous flame. They have the same initial droplet mass loading $\delta = 0.6$. Qualitatively, the distributions of gas temperature and droplet mass loading of flames E and F are respectively similar to the counterpart homogeneous and heterogeneous flames, i.e. A and B. However, different from them, the burned gas temperatures at $\eta = -\infty$ in both cases are considerably below that of the purely gaseous flame. This is justifiable, because the addition of the fuel vapor into the mixture would render rich gaseous composition deviate more from stoichiometry. Particularly, in Flame F, the lower temperature of burned gas also results in larger temperature gradient in the post-flame evaporation zone, as shown in Fig. 4(d), and therefore more heat conduction from the flame. The structures of fuel-rich flames E and F are also similar to those of water-droplet-laden planar flames by Belyakov et al. (2018).

Locations of evaporation onset and completion fronts, η_v and η_c , relative to the flame front can also be analytically determined from our theories in Section 3.2, subject to gas and droplet properties. As seen from Fig. 4, they are considerably different in homogeneous and heterogeneous flames, and differentiate the thermal and kinetic effects of the respective evaporating fuel droplets. Therefore, Fig. 5 generalizes η_v and η_c of droplet-laden flames with different initial droplet size and mass loading. For fuel-lean conditions in Fig. 5(a), the curves are reverse 7-shaped, and it is shown that initial mass loading δ has relatively small effects on η_v and η_c . Moreover, the evaporation onset front η_v is before the flame front and varies little when $d_0 > 10 \mu\text{m}$. However, for $d_0 \leq 10 \mu\text{m}$, η_v slowly decrease with smaller d_0 . This is because for smaller droplets they reach the boiling temperature closer to the flame front. Meanwhile, with increased d_0 , evaporation completion front η_c firstly precedes the flame front and then penetrates across the flame front (i.e. $\eta = 0$) into the post-flame zone. The further droplet penetration is parameterized by increased magnitudes of η_c . Note that crossing the flame front implies the transition from homogenous flame to heterogeneous one, as also can be from Fig. 1. Besides, the length of the evaporation zone increases with d_0 , which can be measured as the relative distance between η_v and η_c , i.e. $|\eta_c - \eta_v|$. In addition, as shown in the inset of Fig. 5(a), asymptotically, when the droplet diameter approaches

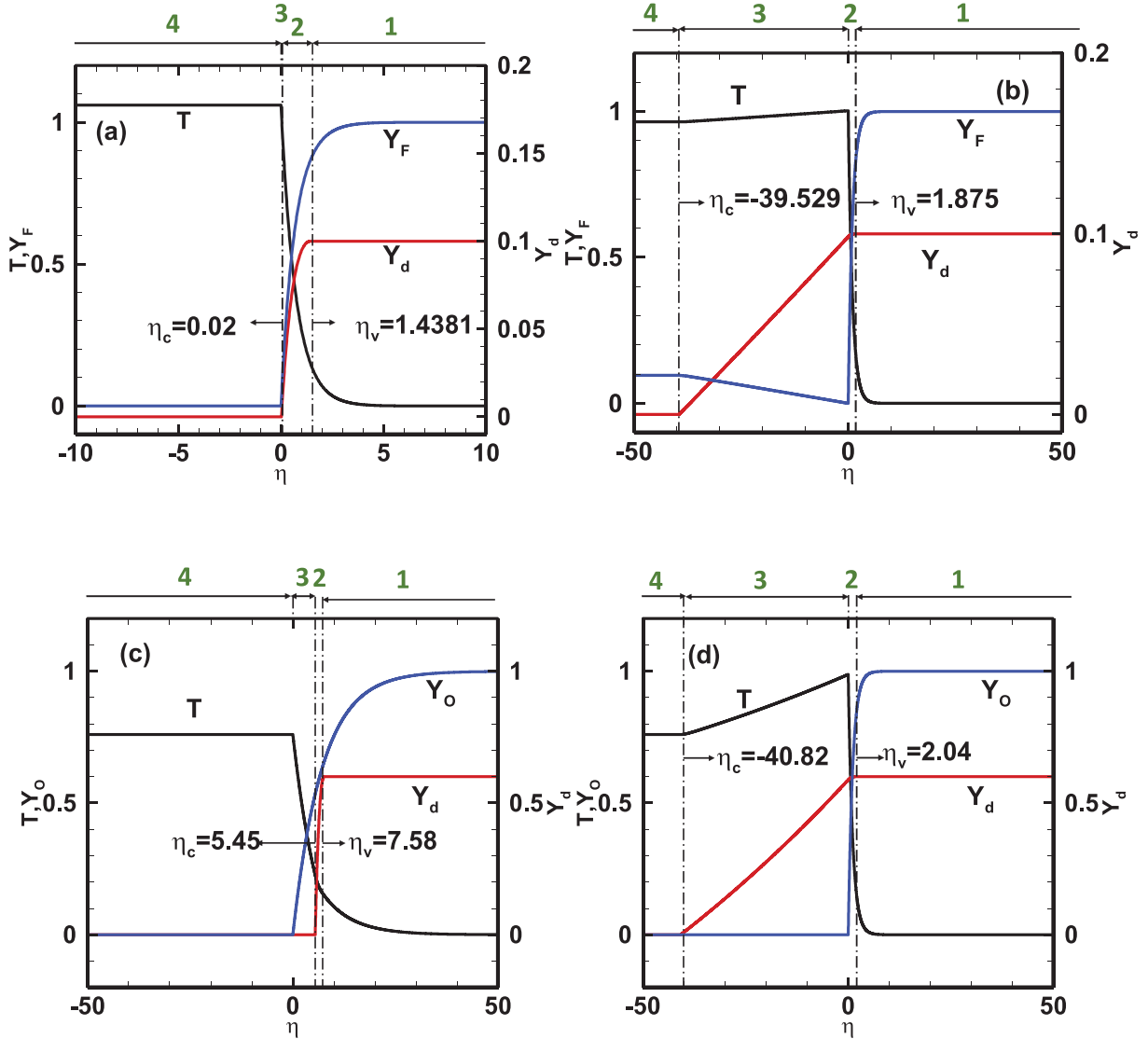


Fig. 4. Structures ($T, Y_{(F,O)}, Y_d$) of four flames: (a) A, (b) B, (c) E and (d) F. They are marked in Figs. 2(a) or 3(a). The dash-dotted lines denote the locations of evaporation onset and completion fronts. The flame front lies at $\eta = 0$. A and E: homogeneous flames; B and F: heterogeneous flames. Green numbers above the upper η -axis indicate the flame / evaporation zones.

zero (i.e. infinitely small droplets), η_v and η_c tend to be equal, due to the infinitely fast evaporation time.

For fuel-rich flames, when the initial mass loadings are small (e.g. $\delta = 0.1$ or 0.4) the curves of η_v and η_c versus initial droplet diameter are qualitatively similar to those from fuel-lean flames. Nevertheless, bifurcation of droplet evaporation front locations, η_v and η_c , can be observed from Fig. 5(b) with larger δ (e.g. 0.6), characterized by Z-shaped curves and consistent with the concurrent bifurcations of flame propagation speed and temperature discussed in Fig. 3. Note that the upper (lower) branch of Z-shaped η_v curve corresponds to the upper (lower) branch of Z-shaped η_c curve. For ease to reference back to Fig. 3, we mark the corresponding turning points C_1, C_2, D_1 and D_2 in Fig. 5(b). For the heterogeneous $C_1 - D_1$ branch, with increased d_0 , η_v is marginally affected, but the norm of η_c increases considerably, indicating larger burned zone with evaporating droplets. As such, the length of evaporation zone increases accordingly. For the upper $C_2 - D_2$ branch, they are mixed with the homogeneous and heterogeneous flames, demarcated by the intersection point at $\eta = 0$. When d_0 approaches

zero, η_v and η_c are asymptotically equal, which is also seen in Fig. 5(a). As d_0 increases, the evaporation zone increased, but when d_0 is slightly beyond $20 \mu\text{m}$, the heterogeneous flame bifurcates: η_v moves closer to the flame, and η_c lies well behind the flame front.

4.2. Effects of latent heat of vaporization

In the last section, the latent heat of vaporization q_v is fixed to be 0.4 . In reality, different liquid fuels have different values of latent heat of vaporization (Lefebvre and McDonell, 2017). Therefore, Figs. 6 and 7 show the flame propagation speed as a function of the initial droplet diameter with $q_v = 0.8$ and 1.2 , respectively. These values correspond to those of liquid fuels with high latent heat, e.g. methanol. Both fuel-lean and fuel-rich flame results are presented. For $q_v = 0.8$, when the droplet diameter and mass loading are fixed (e.g. $d_0 = 5 \mu\text{m}$ and $\delta = 0.2$), the propagation speed U is lower and therefore closer to that of the droplet-free flame, compared to the results with $q_v = 0.4$ in Figs. 2 and 3. This indicates that the flame enhancement under fuel-lean con-

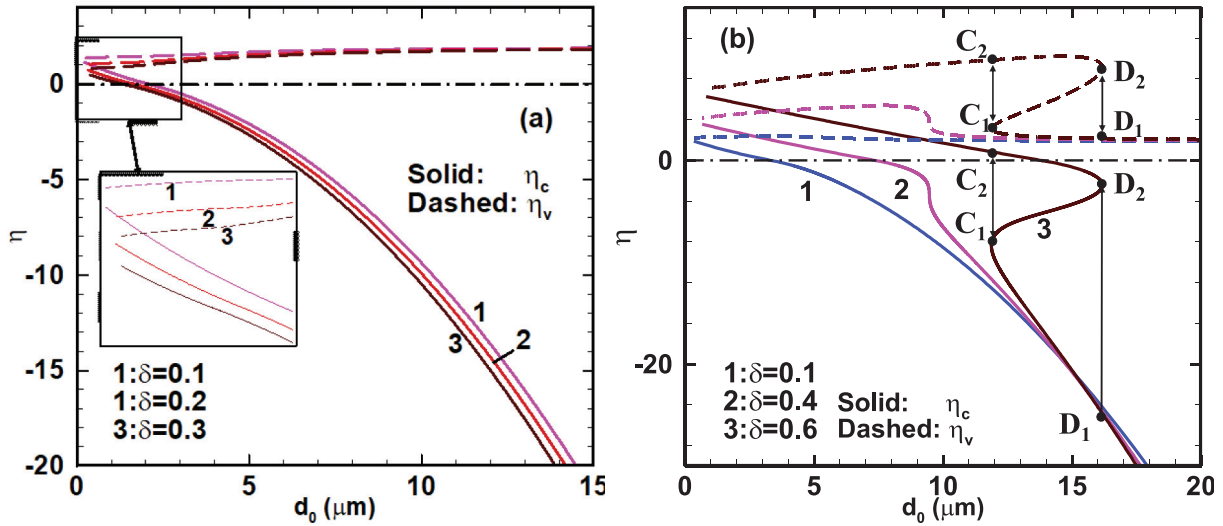


Fig. 5. Evaporation onset and completion fronts versus initial droplet diameter: (a) fuel-lean (b) fuel-rich conditions. The dash-dotted lines are flame front, i.e. $\eta = 0$, the bi-arrow lines show the flame bifurcation in the labeled points. C_1 , C_2 , D_1 and D_2 are consistent with the corresponding points in Fig. 3(a).

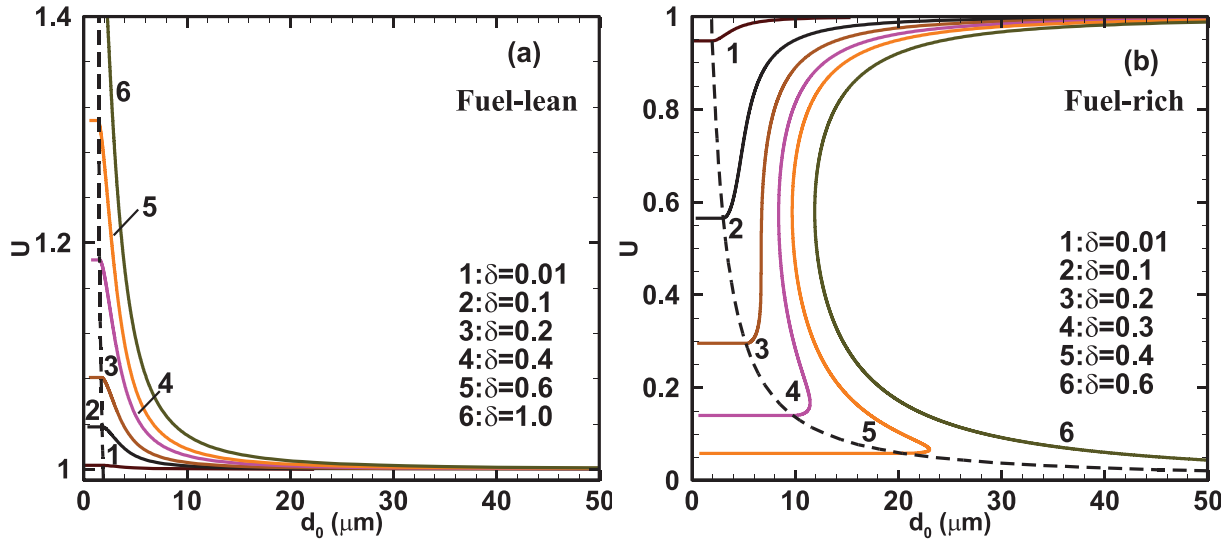


Fig. 6. Effect of droplet diameter and mass loading on the flame propagation speed for $q_v = 0.8$: (a) fuel-lean, (b) fuel-rich. Homogeneous (heterogeneous) flames: left (right) to the dashed flame regime line.

dition is weakened. This may be due to more heat absorbed from the gas phase to vaporize the fuel droplets. However, for the fuel-rich case in Fig. 6(b), when the flame is locally homogeneous, the flame propagation speed is lower for the same d_0 and δ (e.g. $d_0 = 5 \mu\text{m}$ and $\delta = 0.2$) when q_v is 0.8, compared to the results with $q_v = 0.4$ in Figs. 2 and 3. Meanwhile, bifurcation of U occurs with smaller δ compared to the results in Fig. 3. As such, for the same droplet mass loading under which bifurcation occurs e.g. $\delta = 0.4$ in Fig. 3(b) and Fig. 6(b), both upper and lower stable branches tend to obtain smaller flame speed for same d_0 when q_v increased from 0.4 to 0.8.

When q_v is further increased to 1.2, the flame propagation speed is below that of the gaseous flames, i.e. $U = 1$ for both fuel-lean and fuel-rich conditions as shown in Figs. 7(a) and 7(b). The results in Fig. 7(a) are different from other fuel-lean results as discussed in Figs. 2 and 7(a), due to the dominance of evaporative heat loss over the kinetic enhancement effects.

4.3. Critical condition for homogeneous and heterogeneous flames

Plotted in Fig. 8 are the flame regime lines in the plane of $U - d_0$ between the homogeneous and heterogeneous flames. Various droplet properties, including initial droplet diameter d_0 and latent heat of vaporization q_v , are considered. Like the flame regime lines in Figs. 2, 3, 6 and 7, each curve in Fig. 8 is calculated using Eqs. (50) - (53) based on a fixed mass loading. In the $U - d_0$ plane here, the left part to each regime line corresponds to homogeneous flames, whilst the right part heterogeneous ones. With decreased q_v from 0.2 to 0.8, the range of the initial droplet diameters where homogeneous flames exist is extended, for both fuel-lean (i.e. $U \geq 1$) and fuel-rich (i.e. $U \leq 1$) flames. Different from the above cases, when q_v is increased to 1.2, no solutions exist beyond $U = 1$, and both regime lines of fuel-lean and fuel-rich conditions are below unity.

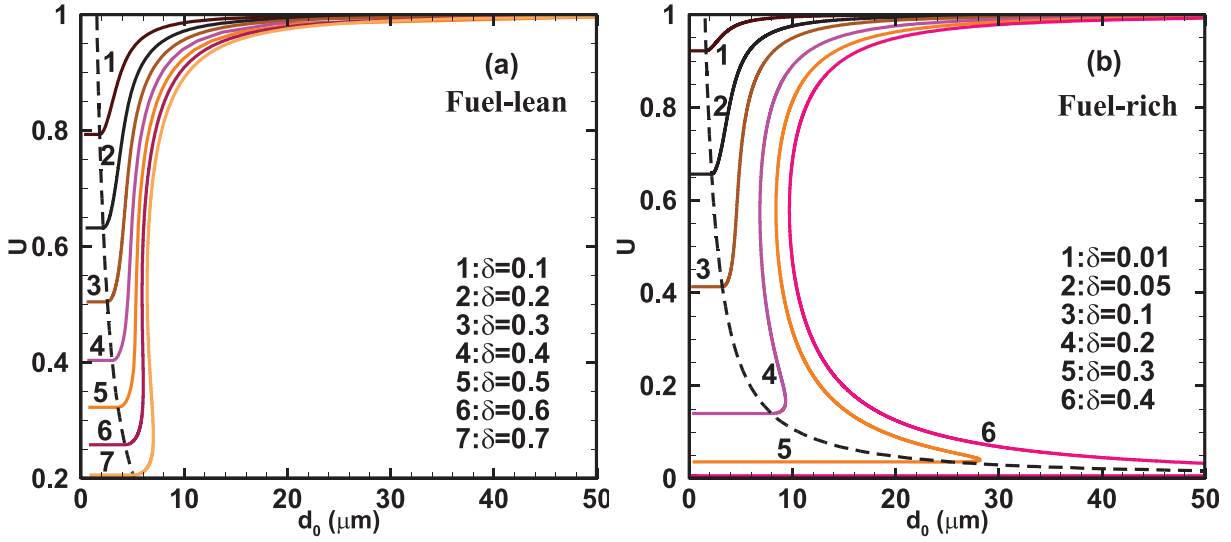


Fig. 7. Effect of droplet diameter and mass loading on the flame propagation speed for $q_v = 1.2$: (a) fuel-lean, (b) fuel-rich. Homogeneous (heterogeneous) flames: left (right) to the dashed flame regime line.

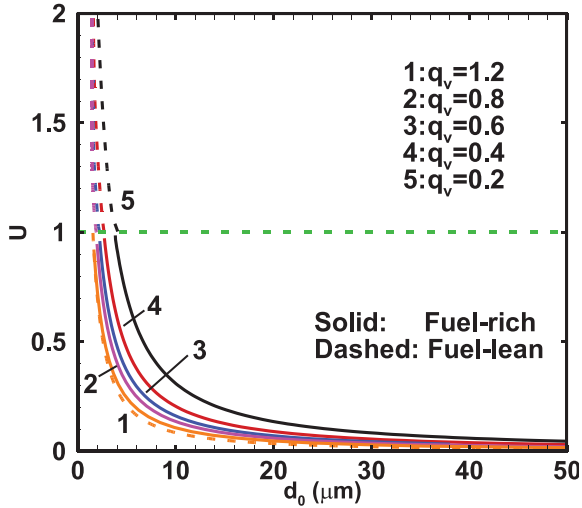


Fig. 8. Effect of fuel latent heat and droplet diameter on the flame regime lines (homogeneous flame: left to the line, heterogeneous flame: right to the line).

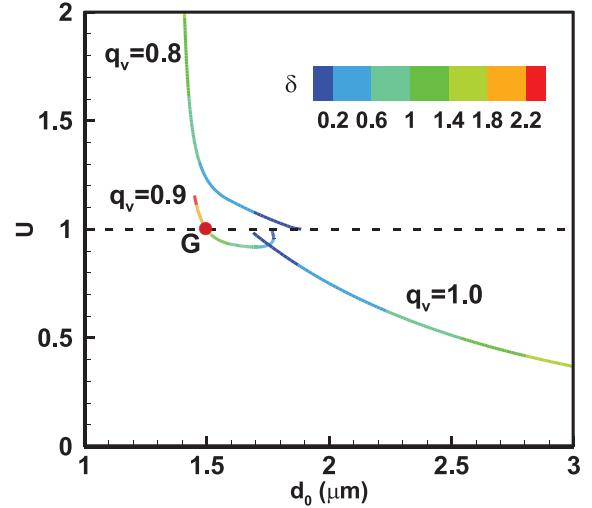


Fig. 9. Effect of fuel latent heat and droplet diameter on flame regime line for fuel-lean condition (homogeneous flame: left to the line, heterogeneous flame: right to the line).

To further identify the critical latent heat of vaporization with which the regime lines critically cross the flame front, Fig. 9 further shows the critical regime curves for fuel-lean flames with latent heat of vaporization $q_v = 0.8, 0.9$ and 1.0 . For $q_v = 0.8$ and 1.0 , their flame propagation speeds U are respectively consistently higher and lower than that of the droplet-free flame (i.e. $\delta = 0$ seen from Fig. 9), i.e. $U = 1$. They respectively correspond to the fact that the flames are overall enhanced and weakened due to the liquid droplets. However, when $q_v = 0.8$, the regime line is firstly (with small mass loading) below the line of $U = 1$. When the mass loading δ increases, the critical conditions, i.e. the solutions along the regime line, move towards smaller droplet diameter, but still below $U = 1$. At point G, the propagation speed of the two-phase flame is the same as that of the droplet-free flame, indicating the kinetic and thermal effects caused by the droplet evaporation counterbalance. Further increasing δ leads to regime line in the upper part of the $U - d_0$ plane, corresponding to flame enhancement by the fuel droplets.

4.4. Evaporative heat loss

The heat loss effects of droplet evaporation on homogeneous and heterogeneous flames have been mentioned in Figs. 2, 3 and 4. In this Section, normalized evaporation heat loss, H , is calculated to quantify these effects in the pre-flame and post-flame zones respectively as

$$H_{ub,HT} = \Omega \int_0^{\eta_v} [T_2(\xi) - T_v] d\xi / \left(\left. \frac{dT}{d\eta} \right|_- - \left. \frac{dT}{d\eta} \right|_+ \right), \quad (54)$$

$$H_{ub,HM} = \Omega \int_{\eta_c}^{\eta_v} [T_2(\xi) - T_v] d\xi / \left(\left. \frac{dT}{d\eta} \right|_- - \left. \frac{dT}{d\eta} \right|_+ \right), \quad (55)$$

$$H_{b,HT} = \Omega \int_{\eta_c}^0 [T_3(\xi) - T_v] d\xi / \left(\left. \frac{dT}{d\eta} \right|_- - \left. \frac{dT}{d\eta} \right|_+ \right), \quad (56)$$

$$H_{b,HM} = 0, \quad (57)$$

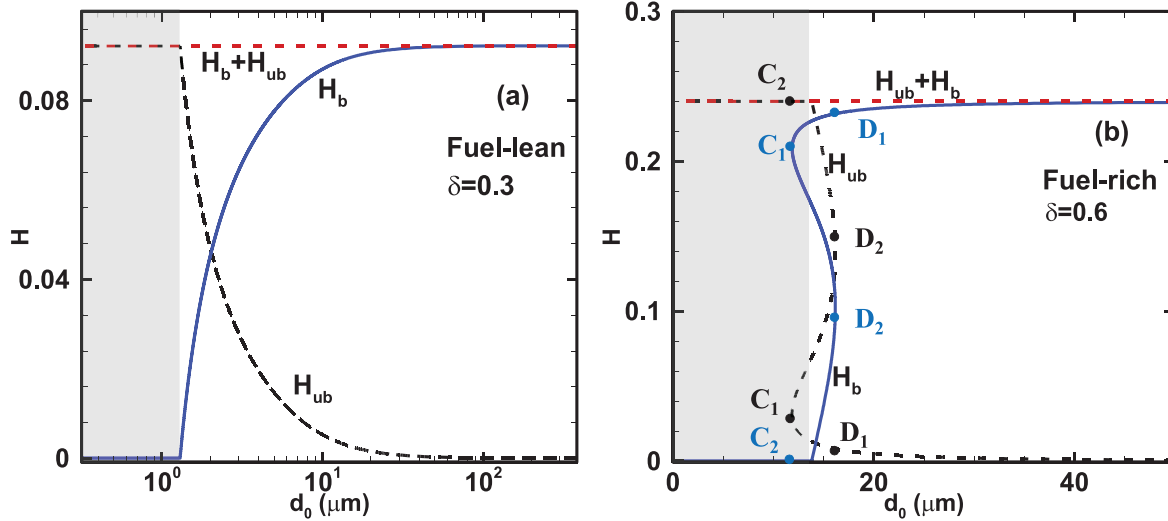


Fig. 10. Normalized evaporation heat loss as a function of initial droplet diameter: (a) $\delta = 0.3$, fuel-lean; (b) $\delta = 0.6$, fuel-rich. $q_v = 0.4$. The shaded area indicates homogeneous flames, while the rest is heterogeneous flame. Points C_1 , C_2 , D_1 and D_2 correspond to the same points in Fig. 3(a).

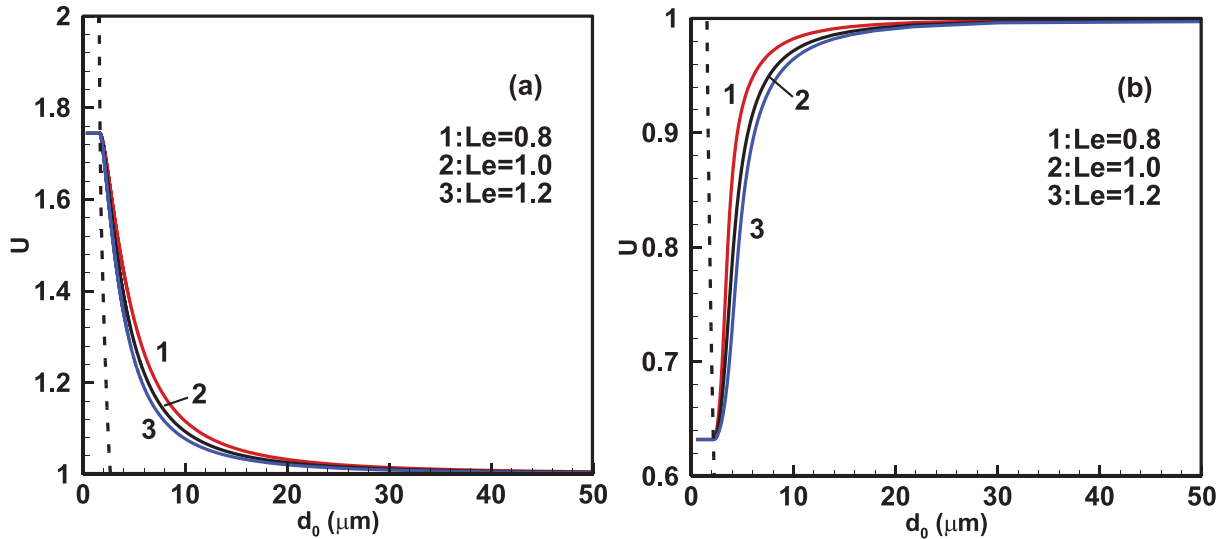


Fig. 11. Effect of the Lewis number and droplet diameter on the flame propagation speed for fuel-lean condition with fixed $\delta = 0.2$ when (a) $q_v = 0.4$, (b) $q_v = 1.2$. Dashed line: flame regime line. Homogeneous flame: left to the dashed line; heterogeneous flame: right to the dashed line.

where the subscripts “ub” and “b” respectively denote pre- and post-flame evaporation zones, whereas “HM” and “HT” respectively denote homogeneous and heterogeneous flames. $\left(\frac{dT}{d\eta}\Big|_- - \frac{dT}{d\eta}\Big|_+\right)$ in the denominator of Eqs. (54) – (56) is the total heat release from the chemical reaction. $T_2(\xi)$ and $T_3(\xi)$ are the temperature distributions in zones 2 and 3, respectively. The integrands, $[T_{[2,3]}(\xi) - T_v]$, indicate the interphase temperature difference in the evaporation zone, where the droplets are at the boiling temperature T_v . Fig. 10 shows the normalized evaporation heat loss (i.e. $H_{ub,HT}$, $H_{b,HT}$, $H_{ub,HM}$ and $H_{b,HM}$) of the selected fuel-lean ($\delta = 0.3$) and fuel-rich ($\delta = 0.6$) flames. Their corresponding flame propagation speeds U as functions of initial droplet diameter d_0 with these two mass loadings have been discussed in Figs. 2 and 3.

Since the initial mass loading δ is constant in all the flame solutions in Figs. 10(a) and 10(b), the sum (i.e. $H_{ub,HT} + H_{b,HT}$, or $H_{ub,HM} + H_{b,HM}$) of evaporative heat loss in their pre- and post-flame zones remains constant, as indicated with the dash-dotted lines. For homogeneous flames (in the shaded area), no droplets are in the burned zone and therefore $H_{b,HM} = 0$, i.e. Eq. (57). More-

over, $H_{ub,HM}$ is constant with d_0 , due to the fixed mass of liquid fuels. For heterogeneous flames, the evaporative heat loss in the pre- and post-flame zones, $H_{ub,HT}$ and $H_{b,HT}$, monotonically decreases and increases with d_0 , respectively. Based on the definitions of mass loading and evaporative heat exchange coefficient, they are correlated through $\Omega \sim \delta/d_0^2$. Therefore, for a constant δ , the larger the droplet diameter d_0 , the slower the evaporative rate and hence smaller heat exchange coefficient Ω . Meanwhile, when d_0 decreases, the interphase temperature difference is reduced as well. Both effects jointly result in monotonic reduction of $H_{ub,HT}$. For post-flame evaporation zone, the high interphase temperature difference leads to gradual increase of $H_{b,HT}$, although Ω decreases, with increased d_0 . When $d_0 > 30 \mu\text{m}$, $H_{ub,HT}$ tends to be zero and the evaporative heat loss is dominantly from the post-flame zone.

Fig. 10(b) shows the normalized evaporative heat loss for selected fuel-rich flames with $\delta = 0.6$. Note that the turning points C_1 , C_2 , D_1 and D_2 correspond to the same points in Fig. 3(a). Solutions of branch $C_1 - D_1$ are strong flames with higher U and T_f , whilst those along $C_2 - D_2$ are weak ones. In the shaded area for homogeneous flames, $H_{b,HM} = 0$, same as those in Fig. 10(a). In

the heterogeneous flames, $H_{ub, HT}$ of branch $C_2 - D_2$ is higher than $H_{b, HT}$. However, for branch $C_1 - D_1$, the tendency is opposite.

4.5. Lewis number effect

Up to this point, the Lewis number is assumed to be $Le = 1$. For fuel-rich flames, the Lewis number is affected by the oxidizer mass diffusion and therefore variations of the Lewis number do not affect the flame propagation speed (results not shown here for brevity). To examine this effect on fuel-lean planar spray flame propagation, Fig. 11 show the flame propagation speed as a function of initial droplet diameter when $Le = 0.8, 1.0$ and 1.2 . The initial droplet loading δ is fixed to be 0.2 . It is seen that propagation speed of homogeneous flame is not dependent on Lewis number for both high and low latent heat. Since the droplet evaporation is completed before the flame front, all the fuel vapor in the pre-flame zone would be depleted by the chemical reaction at the flame front and it behaves like a purely gaseous flame.

For heterogeneous flames, droplet evaporation occurs in the post-flame zone and fuel vapor exists therein, as seen from the structure of heterogeneous flames in Fig. 4(b). In this case, the fuel vapor diffusion considerably influences the consumption at the flame front. Specifically, the smaller (larger) Lewis number indicates a higher (lower) mass diffusivity and therefore more (less) fuel vapor from the post-flame zone can contribute towards the combustion, thereby leading to an enhanced (reduced) flame propagation speed. Note that these are remarkable only for intermediate droplet diameters. For heterogeneous flames laden with relatively small (d_0 slightly larger than $2 \mu\text{m}$) or large ($d_0 > 20 \mu\text{m}$) droplets, dependence of heterogeneous flame propagation speed on Lewis number is minimized. This is because for small droplets, the evaporation completion location η_c in the post-flame zone is close to the flame front and fuel vapor can be consumed locally. Conversely, when the droplet size is large, the post-flame evaporation zone is large, leading to a reduced gradient of fuel vapor from liquid droplets.

5. Conclusions

Propagation of one-dimensional laminar planar flames laden with fuel droplet mists is investigated theoretically. Localized homogeneous and heterogeneous flames are considered, which are characterized by different relative locations of dispersed fuel droplets and flame front. Within the framework of large activation energy, correlations describing flame propagation speed, flame temperature, evaporation onset and completion fronts are derived. With this correlation, the influences of droplet (e.g. diameter and droplet mass loading) and fuel (e.g. latent heat of vaporization) parameters on propagation of fuel-droplet-laden planar flames are assessed.

The results indicate that fuel droplets affect the flame propagation differently for fuel-lean and fuel-rich conditions. Under fuel-lean conditions, the flames are enhanced by the evaporating droplets. The burned gas temperature of homogeneous flame is slightly higher than the purely gaseous flame due to the fuel vapor addition. For fuel-lean heterogeneous flames, residual fuel vapor and considerable temperature gradient exist in the post-flame evaporation zone. However, under fuel-rich conditions, the droplets suppress the flame propagation. The tendencies of temperature and droplet mass loading distributions are similar to those from the fuel-lean cases. However, the burned gas temperature is much lower than that of fuel-lean case, due to the off-stoichiometric compositions. In addition, the foregoing effects on fuel-rich and fuel-lean flames under respective conditions are intensified with increased droplet mass loading.

Our results also show that evaporation completion front location is largely affected by the droplet diameter, instead of mass loading. Conversely, the evaporation onset front varies little with droplet properties. Bifurcation and multiplicity are observed for large droplet loading and fuel-rich gas composition, in terms of the propagation speed and droplet evaporation onset/completion front locations.

It is also shown that for different values of latent heat, the droplet evaporative heat loss effects on the flame propagation are different. This is particularly pronounced for the fuel-lean conditions, where increasing latent heat leads to variations from flame enhancement to weakening relative to the droplet-free flames. The normalized evaporative heat loss in different flame and evaporation zones are also calculated. In general, for homogeneous flames, the heat loss only occurs in the pre-flame zone. However, for heterogeneous flames, heat loss in the post-flame evaporation zone become dominant for relatively large droplets. Furthermore, the effect of Lewis number on laminar planar spray flames is also studied, and it is found that Lewis number influences heterogeneous flame propagation speed under fuel-lean conditions when the droplet diameter is intermediate.

Declaration of Competing Interest

None.

CRediT authorship contribution statement

Qiang Li: Conceptualization, Methodology, Validation, Formal analysis, Writing - original draft, Visualization. **Huangwei Zhang:** Conceptualization, Methodology, Writing - review & editing, Supervision, Project administration, Funding acquisition. **Chang Shu:** Writing - review & editing, Supervision.

Acknowledgement

QL are financially supported by Research Scholarship Budget from National University of Singapore (NUS). HZ is financially supported by the start-up grant (R-265-000-604-133) from NUS.

Supplementary materials

Supplementary material associated with this article can be found, in the online version, at doi:[10.1016/j.ijmultiphaseflow.2020.103452](https://doi.org/10.1016/j.ijmultiphaseflow.2020.103452).

References

- Aggarwal, S.K., Sirignano, W.A., 1985. Unsteady spray flame propagation in a closed volume. *Combust. Flame* 62, 69–84.
- Atzler, F., Demoulin, F.X., Lawes, M., Lee, Y., Marquez, N., 2006a. Burning rates and flame oscillations in globally homogeneous two-phase mixtures (flame speed oscillations in droplet cloud flames). *Combust. Sci. Technol.* 178, 2177–2198.
- Atzler, F., Lawes, M., Sulaiman, S.A., Woolley, R., 2006b. Effects of droplets on the flame speed of laminar iso-octane and air aerosols. 10th Int. Conf. Liq. At. Spray Syst ICLASS 2006.
- Ballal, D.R., Lefebvre, A.H., 1981. Flame propagation in heterogeneous mixtures of fuel droplets, fuel vapor and air. *Symp. Combust.* 321–328.
- Belyakov, N.S., Babushok, V.I., Minaev, S.S., 2018. Influence of water mist on propagation and suppression of laminar premixed flame. *Combust. Theory Model.* 22, 394–409.
- Blouquin, R., Cambay, P., Joulin, G., 1997. Radiation-affected dynamics of enclosed spherical flames propagating in particle-laden premixtures. *Combust. Sci. Technol.* 128, 231–255.
- Blouquin, R., Joulin, G., 1995. Radiation-affected hydrodynamic instability of particle-laden flames. *Combust. Sci. Technol.* 110–111, 341–359.
- Bradley, D., Lawes, M., Liao, S., Saat, A., 2014. Laminar mass burning and entrainment velocities and flame instabilities of i-octane, ethanol and hydrous ethanol/air aerosols. *Combust. Flame* 161, 1620–1632.
- Chen, Z., Ju, Y., 2007. Theoretical analysis of the evolution from ignition kernel to flame ball and planar flame. *Combust. Theory Model.* 11, 427–453.

- Continillo, G., Sirignano, W.A., 1989. Numerical study of multicomponent fuel spray flame propagation in a spherical closed volume. *Symp. Combust.* 1941–1949.
- Greenberg, J.B., 2007. Finite-rate evaporation and droplet drag effects in spherical flame front propagation through a liquid fuel mist. *Combust. Flame* 148, 187–197.
- Greenberg, J.B., McIntosh, A.C., Brindley, J., 2001. Linear stability analysis of laminar premixed spray flames. *Proc. R. Soc. London. Ser. A Math. Phys. Eng. Sci.* 457, 1–31.
- Han, W., Chen, Z., 2016. Effects of finite-rate droplet evaporation on the extinction of spherical burner-stabilized diffusion flames. *Int. J. Heat Mass Transf.* 99, 691–701.
- Han, W., Chen, Z., 2015. Effects of finite-rate droplet evaporation on the ignition and propagation of premixed spherical spray flame. *Combust. Flame* 162, 2128–2139.
- Hayashi, S., Kumagai, S., 1975. Flame propagation in fuel droplet-vapor-air mixtures. *Symp. Combust.* 445–452.
- Hayashi, S., Kumagai, S., Sakai, T., 1977. Propagation Velocity and Structure of Flames in Droplet-Vapor-Air Mixtures. *Combust. Sci. Technol.* 15, 169–177.
- He, L., 2000. Critical conditions for spherical flame initiation in mixtures with high Lewis numbers. *Combust. Theory Model.* 4, 159–172.
- Joulin, G., 1981. Asymptotic analysis of non-adiabatic flames: heat losses towards small inert particles. *Symp. Combust.* 18, 1395–1404.
- Joulin, G., Clavin, P., 1979. Linear stability analysis of nonadiabatic flames: diffusion-thermal model. *Combust. Flame* 35, 139–153.
- Ju, Y., Law, C.K., 2000. Dynamics and extinction of non-adiabatic particle-laden premixed flames. *Proc. Combust. Inst.* 28, 2913–2920.
- Lefebvre, A.H., McDonell, V.G., 2017. *Atomization and Sprays*. CRC press.
- Li, H., Zhang, H., Chen, Z., 2018. Effects of endothermic chain-branching reaction on spherical flame initiation and propagation. *Combust. Theory Model.* 1–19.
- Li, Q., Liu, C., Zhang, H., Wang, M., Chen, Z., 2020. Initiation and propagation of spherical premixed flames with inert solid particles. *Combust. Theory Model.* 1–26.
- Lin, T.-H., Law, C.K., Chung, S.H., 1988. Theory of laminar flame propagation in off-stoichiometric dilute sprays. *Int. J. Heat Mass Transf.* 31, 1023–1034.
- Lin, T.-H., Sheu, Y.Y., 1991. Theory of laminar flame propagation in near-stoichiometric dilute sprays. *Combust. Flame* 84, 333–342.
- Liu, C.-C., Lin, T.-H., 1991. The interaction between external and internal heat losses on the flame extinction of dilute sprays. *Combust. Flame* 85, 468–478.
- Liu, C.C., Lin, T.-H., Tien, J.H., 1993. Extinction theory of stretched premixed flames by inert sprays. *Combust. Sci. Technol.* 91, 309–327.
- Mitani, T., 1981. A flame inhibition theory by inert dust and spray. *Combust. Flame* 43, 243–253.
- Myers, G.D., Lefebvre, A.H., 1986. Flame propagation in heterogeneous mixtures of fuel drops and air. *Combust. Flame* 66, 193–210.
- Neophytou, A., Mastorakos, E., 2009. Simulations of laminar flame propagation in droplet mists. *Combust. Flame* 156, 1627–1640.
- Nicoli, C., Haldenwang, P., Suard, S., 2005. Analysis of pulsating spray flames propagating in lean two-phase mixtures with unity Lewis number. *Combust. Flame* 143, 299–312.
- Nomura, H., Izawa, K., Ujiie, Y., Sato, J., Marutani, Y., Kono, M., Kawasaki, H., 1998. An experimental study on flame propagation in lean fuel droplet-vapor-air mixtures by using microgravity conditions. *Symp. Combust.* 2667–2674.
- Nomura, H., Kawasumi, I., Ujiie, Y., Sato, J., 2007. Effects of pressure on flame propagation in a premixture containing fine fuel droplets. *Proc. Combust. Inst.* 31, 2133–2140.
- Nomura, H., Koyama, M., Miyamoto, H., Ujiie, Y., Sato, J., Kono, M., Yoda, S., 2000. Microgravity experiments of flame propagation in ethanol droplet-vapor-air mixture. *Proc. Combust. Inst.* 28, 999–1005.
- Ranz, W.E., W. R. Marshall, J., 1952. Evaporation from Drops. Part I. *Chem. Eng. Prog.* 48, 141–146.
- Sacomano Filho, F.L., Speelman, N., van Oijen, J.A., de Goey, L.P.H., Sadiki, A., Janicka, J., 2018. Numerical analyses of laminar flames propagating in droplet mists using detailed and tabulated chemistry. *Combust. Theory Model.* 22, 998–1032.
- Sazhin, S.S., 2006. Advanced models of fuel droplet heating and evaporation. *Prog. Energy Combust. Sci.* 32, 162–214.
- Seth, B., Aggarwal, S.K., Sirignano, W.A., 1980. Flame propagation through an air-fuel spray mixture with transient droplet vaporization. *Combust. Flame* 39, 149–168.
- Sulaiman, S.A., 2006. *Burning Rates and Instabilities in the Combustion of Droplet and Vapour Mixtures*. The University of Leeds.
- Sulaiman, S.A., Lawes, M., Atzler, F., Woolley, R., 2007. Effects of droplets on the flame speed of laminar Iso-octane and air aerosols. *Mission. Res. Petrochemical Catal. Technol.*
- Thimothée, R., Chauveau, C., Halter, F., Gökalp, I., 2017a. Experimental investigation of the passage of fuel droplets through a spherical two-phase flame. *Proc. Combust. Inst.* 36, 2549–2557.
- Thimothée, R., Chauveau, C., Halter, F., Nicoli, C., Haldenwang, P., Denet, B., 2017b. Microgravity experiments and numerical studies on ethanol/air spray flames. *Comptes Rendus Mécanique* 345, 99–116.
- Zhang, H., Chen, Z., 2011. Spherical flame initiation and propagation with thermally sensitive intermediate kinetics. *Combust. Flame* 158.
- Zhang, H., Guo, P., Chen, Z., 2013. Critical condition for the ignition of reactant mixture by radical deposition. *Proc. Combust. Inst.* 34, 3267–3275.
- Zhuang, Y., Zhang, H., 2020. On flame bifurcation and multiplicity in consistently propagating spherical flame and droplet evaporation fronts. *Int. J. Multiph. Flow* 125, 103220.
- Zhuang, Y., Zhang, H., 2019. Effects of water droplet evaporation on initiation, propagation and extinction of premixed spherical flames. *Int. J. Multiph. Flow* 117, 114–129.